Detection of condensed-phase explosives via laser-induced vaporization, photodissociation, and resonant excitation

C. M. Wynn,* S. Palmacci, R. R. Kunz, K. Clow, and M. Rothschild

Lincoln Laboratory, Massachusetts Institute of Technology, 244 Wood Street, Lexington, Massachusetts 02420, USA

*Corresponding author: cwynn@ll.mit.edu

Received 20 May 2008; revised 22 August 2008; accepted 11 September 2008;
posted 17 September 2008 (Doc. ID 96460); published 23 October 2008

We investigate the remote detection of explosives via a technique that vaporizes and photodissociates the condensed-phase material and detects the resulting vibrationally excited NO fragments via laser-induced fluorescence. The technique utilizes a single 7 ns pulse of a tunable laser near 236.2 nm to perform these multiple processes. The resulting blue-shifted fluorescence (226 nm) is detected using a photomultiplier and narrowband filter that strongly block the scatter of the pump laser off the solid media while passing the shorter wavelength photons. Various nitro-bearing compounds, including 2,6-dinitrotoluene (DNT), 2,4,6-trinitrotoluene (TNT), pentaerythritol tetranitrate (PETN), and hexahydro-1,3,5-trinitro-1,3,5-triazine (RDX) were detected with a signal-to-noise of 25 dB. The effects of laser fluence, wavelength, and sample morphology were examined.

OCIS codes: 300.2530, 280.3420, 280.0280, 190.4180.

1. Introduction

The development of a technique with the ability to detect trace quantities of explosives at a distance is of great interest [1]. In numerous situations, when explosive devices are prepared, transported, or otherwise handled, certain amounts of the explosive material end up on surfaces. It would be of great interest to detect these chemical residues, as they would serve as indicators for attempts at concealed assembly or transport of explosive materials and devices. Any proposed detection technique of such traces must simultaneously satisfy two fundamental, yet often contradictory, requirements: it must be sensitive enough to rapidly detect trace amounts of the target compound at a distance, and it must be as immune as possible to false alarms generated by the naturally occurring complex environments in which these trace explosives may be found. Several methods for standoff detection of explosive residues have been under investigation, the most prominent being laser-induced breakdown spectroscopy (LIBS) and Raman spectroscopy. However, to date neither LIBS nor Raman has demonstrated satisfactory performance in *both* categories [1,2]. While future improvements in LIBS and Raman, and even the implementation of a combination of the two, are possible, alternative standoff detection methods need to be explored. A promising method is based on the use of photodissociation followed by laser-induced fluorescence (PD-LIF). Strictly speaking, PD-LIF operates on the vapor phase of a material. However, since the vapor pressure of most explosives is so low (see Table 1), a vaporization step of the solid residues is virtually a necessity in order to access as many molecules as possible. Our approach is to perform vaporization of the sample in addition to PD-LIF. This approach of vaporization/PD-LIF in the context of standoff explosives detection, requires the near-simultaneous occurrence of the following steps (Fig. 1): (1) vaporization of the explosive molecules residing at or near a surface; (2) photo-induced dissociation of the explosive molecules, generating appropriate photofragments; (3) resonant excitation of the

0003-6935/08/315767-10$15.00/0

Table 1. Structures and Physical Properties of Compounds under Study[a]

Compound	Molecular Structure	Vapor Pressure at 300 K (ppb)	R–NO_2 Bond Energy (kcal/mol)	Absorbance at 236.2 nm (cm^2/molecule)
DNT	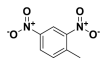	~200	70.6[b]	5.0×10^{-17}
TNT	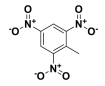	13	33.61	7.7×10^{-17}
RDX	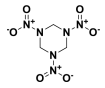	0.0084	23.64	4.3×10^{-17}
PETN	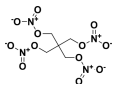	0.026	20.00	5.4×10^{-18}

[a]Vapor pressure data are for the solid phases and are from [21] for DNT and [22] for TNT, RDX, and PETN. Absorbance cross sections were measured in this study. Bond scission energies (with the exception of DNT) were calculated in [18].

[b]Note that measurements [23] of DNT indicate the highest bond scission energy (70.6 kcal/mol); however, these results do not appear consistent with the calculations for the other compounds.

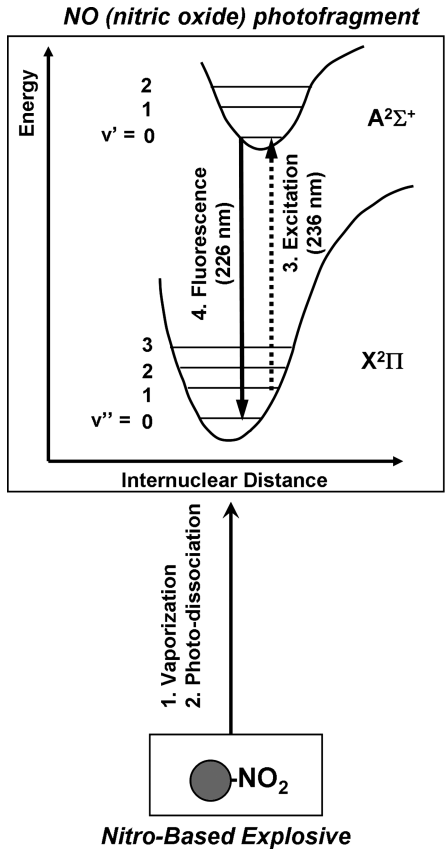

Fig. 1. Schematic of steps and energy levels associated with the vaporization/PD-LIF detection process. Solid explosives (bottom of figure) are vaporized and dissociated into diatomic NO fragments in the first two (simultaneous) steps. The resultant NO fragments (top of figure) are optically excited (Step 3) from their vibrationally excited electronic ground state to an electronically excited state. The blue-shifted fluorescence (Step 4) is used for detection.

photofragments; and (4) fluorescence from the excited state of the photofragments, to be detected by a suitable optical system.

There have been encouraging reports that PD-LIF of nitro-bearing explosive compounds in their vapor phase is indeed feasible (Steps 2–4 above). Specifically the ultraviolet (UV)-induced photodissociation of molecules such as trinitrotoluene (TNT) has been shown to form fragments, including the diatomic NO, at various levels of rotational and vibrational excitation of its electronic ground state ($X^2\Pi$). Thus Step 3 above, resonant photoexcitation of NO, can be accomplished at several wavelengths, depending on the choice of lower and upper molecular energy levels. Transitions to the electronic excited state $A^2\Sigma$ are in the UV, and the resultant radiative decay back to the $X^2\Pi$ state (Step 4 above) would also be in the UV. In order to increase the sensitivity of detection, it would be preferable to excite the vibrational state that has the highest nascent population following photodissociation. This is the vibrational ground state, $v'' = 0$. However, excitation of $v'' = 0$ leads to fluorescence either at the excitation wavelength itself or at wavelengths longer than the excitation wavelength, both scenarios leading to increased risk of false alarms. At the laser wavelength, scattered photons from the exciting laser will swamp any fluorescence from NO; false alarms may also be generated by atmospheric NO, which exists in the vibrational ground state under ambient conditions. At wavelengths longer than the excitation wavelength, many naturally occurring compounds will exhibit similar UV-induced fluorescence (including atmospheric NO and NO_x). One strategy to overcome this problem is to probe $v'' > 0$ states, since now some of the fluorescence will take place at wavelengths shorter than the excitation wavelength, and this is an unusual enough occurrence under normal circumstances to significantly reduce the probability of false alarms. Note that Boltzmann statistics predict that the $v'' = 1$ state of NO will have a relative population of $\sim 10^{-5}$ at room temperature. Excitation of $v'' > 0$ states is, of course, predicated on the assumption that these states are populated to some degree when the parent molecule is dissociated.

In recent years, a number of promising experiments have demonstrated the potential of this approach. PD-LIF measurements of TNT in vapor formed in the UV showed clear evidence of vibrationally excited NO, and excitation of NO in its $v'' = 2$ state at 248 nm resulted in fluorescence [3,4]. The formation of the vapor phase was accomplished by heating the solid or by other means [5].

We report an all-optical technique for the detection of condensed phases of nitro-bearing explosives, thus allowing truly remote detection. We utilize a single UV laser to perform the first three steps listed above

(vaporization, photodissociation, and excitation). Additionally we focus our studies primarily on the excitation of NO fragments from their first vibrationally excited state ($v'' = 1$), because this state has the highest population other than $v'' = 0$ [6]. For these states the excitation wavelength is ~236 nm, while the detected fluorescence is at ~226 nm (Fig. 1).

2. Experimental

The three main components in single-laser PD-LIF laboratory experiments are (Fig. 2) the excitation laser, the detection optics, and the samples being tested. In our studies the laser was a tunable, pulsed Continuum 9030 system, which frequency triples a Nd:YAG source and inputs the 355 nm result into an optical parametric oscillator (OPO) providing frequency tunability. The output of the OPO is subsequently frequency doubled, providing variable laser output from 215 to 310 nm. The laser output was an ~1 cm^2 beam of 30 Hz pulses with energies of 2–3 mJ per pulse and pulse widths of ~7 ns. The spectral linewidth was 0.03–0.04 nm near the wavelengths of interest. The absolute values of the laser wavelengths were confirmed using an Ocean Optics spectrometer, which was calibrated with a Hg discharge lamp. All wavelengths reported are in air. *In situ* measurements of the laser power were recorded using a Molectron power meter and pyrometer-based measurement head; laser power fluctuations during a typical measurement were approximately 10%.

The fluorescence detection subsystem consisted of a solar blind photomultiplier tube (PMT) with narrowband filters. The PMT was a Perkin Elmer Cs–Te channel photomultiplier with negligible dark counts (measured to be ~4 per minute), single photon sensitivity, and quantum efficiency of 10% near the signals of interest (220–230 nm). The PMT signal was amplified using a 5 kHz preamplifier, and the resulting signal was recorded using an analog-to-digital converter and computer. The PMT was used

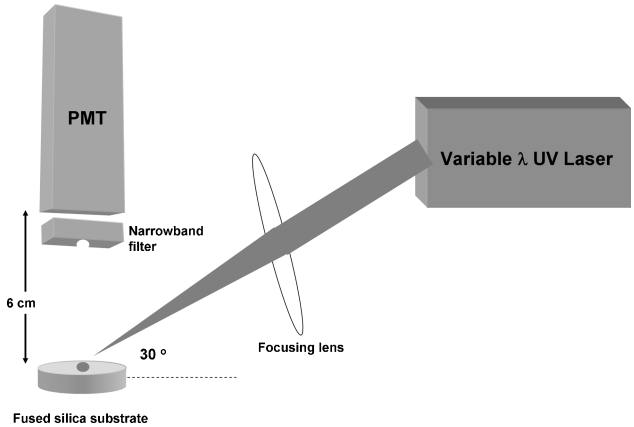

Fig. 2. Experimental detection setup. The primary components used were a variable-wavelength pulsed UV laser (the light from which was focused on the sample with a UV lens), a narrowband filter strongly rejecting the laser scatter, and a PMT photodetector. The explosive samples were placed on fused silica substrates.

in both a photon-counting and linear mode, dependent upon photon flux. It was calibrated for short laser pulses at various cathode voltages in order to ensure a linear response at a given flux level.

Narrowband filters are essential in these experiments, as they are needed to suppress the scattered laser light. The filters that we used consisted of fused silica substrates with a dielectric film stack coating designed by Barr Associates. The total transmission of the three-filter stack used in these measurements was 0.3% [optical density (OD) 2.5] at the signal wavelength of 226 nm and OD 11 at the primary laser wavelength of 236 nm, providing a rejection ratio of nearly nine orders of magnitude between the laser and the expected signal.

Experiments were performed primarily in close-range geometry so that the PMT and filters were positioned 6 cm directly above the sample. No collection or collimation optics were used in the close-range configuration. In this geometry the following estimates can be made regarding signal collection efficiency. Assuming the signal fluoresces in an isotropic manner, and using the 0.3% transmission of the filters at the signal wavelength of 226 nm, the 0.25″ detector aperture, the detection range of 6 cm, and the quantum efficiency of 10%, we estimate a collection efficiency of 4×10^{-7} of all emitted signal photons. While this proof-of-concept laboratory detector did not have optimal collection efficiency, we believe that, in general, interference-based filters offer the most promise for the explosives detection process. The 0.3% efficiency of our filter stack is currently being improved by Barr Associates with expectations of transmission as high as 25% (while retaining the high rejection). In contrast, an etalon-based filtering approach attempted by TecOptics failed to achieve even 0.3% transmission, largely due to difficulties with material absorption. A monochromator-based technique was also considered as a means of optical filtering. However, the monochromator throughput is expected to be worse than that of the current filters since the high rejection requirements dictate either a dual or triple grating system with a fairly large path length (likely greater than 0.5 m) and relatively narrow slit width (less than ~1 mm). The overall throughput of such a combination is expected to be worse than our current filter transmission.

The laser beam was focused with a convex UV lens on an ~0.1 cm^2 spot at the sample, at an incident angle of ~60° from the normal. The spot size was estimated by exposing photoresist to the UV illumination at the sample location and measuring the resultant spot.

A variety of explosives in a variety of morphologies were studied. Structures, and some of their relevant physical properties, are displayed in Table 1. The explosives included 2,6-dinitrotoluene (DNT), TNT, pentaerythritol tetranitrate (PETN), and hexahydro-1,3,5-trinitro-1,3,5-triazine (RDX). DNT, as received from Aldrich, was in the form of small

granules, roughly the size of salt crystals. Studies were performed on macroscopic mounds (several milligrams) of these solid granules, in addition to a liquid form that was obtained by heating the granules to 80 °C. With the exception of the liquid DNT measurements, all other measurements were performed at room temperature under ambient atmospheric conditions. Military-grade TNT was studied in a solid pellet form. Additionally, TNT was dropcast from a dilute acetone solution to form a thin film containing a calibrated amount (1 μg) of TNT residue on a silicon wafer. Military-grade PETN was studied in the form of a white powder. RDX was studied both as a trace coating on sand (8% by weight) and as the dominant component (~90%) in the putty-like C4 plastic explosive. In all morphologies the experimentally observed signal remained essentially the same, with only variations in the signal magnitude and effective rotational temperature as will be discussed in Section 3. Irradiation of the explosives caused a visible discoloration to a brownish color. For macroscopic samples the signal did not vary significantly with a cumulative dose, while with the dropcast sample it disappeared after 10–30 pulses, as the material was being used up in the photodissociation process (see also Section 3).

Solution-phase absorption spectra were collected using a Hitachi U-4001 UV-visible spectrophotometer, and 10 μM solutions were prepared using samples of DNT, TNT, RDX, and PETN dissolved in spectrophotometric-grade acetonitrile. Samples were measured in UV-grade fused silica cuvettes with optical paths of 1 cm.

3. Results and Discussion

Absorption of the incident UV light is an essential first step in the dissociation process. Absolute cross sections for this process for the four materials under study were deduced using a UV-visible spectrophotometer that measured the absorption of known quantities of material over a spectral range of 190–590 nm. Figure 3 displays the cross sections as a function of wavelength. It should be noted that these are solution-phase cross sections, which differ somewhat from the solid-phase cross sections. However, the overall features of the solution-phase cross sections are expected to be similar to those of the solid phase. All materials show little to no absorption in the visible, with the onset of absorption beginning below ~300 nm. TNT has the strongest absorption at 236 nm, while PETN has the weakest. Values of the cross sections at 236 nm are also reported in Table 1.

Figure 4 displays the results of close-range fluorescence detection measurements of DNT, TNT, C4 (RDX being the active component), and PETN. All samples were in bulk quantities placed on UV-grade fused silica substrates. For these measurements the incident laser was scanned from 235 to 238 nm in 0.01 nm steps. Data were taken at a fluence of 10 mJ/cm^2/pulse (1 mJ pulses over a 0.1 cm^2 area). In Figs. 4(a)–4(d) and in the background measure-

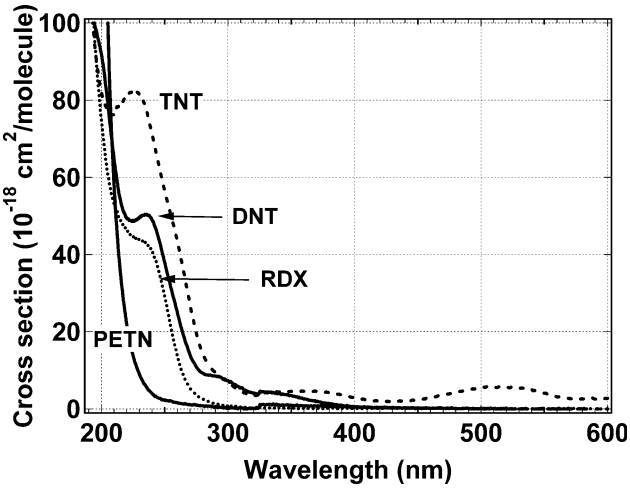

Fig. 3. Absorption cross section as a function of wavelength for explosives in acetonitrile solutions.

ments of Fig. 4(e), the laser directly illuminated the samples. In contrast the vapor DNT data of Fig. 4(e) were collected by focusing the beam ~3 mm above the liquid DNT sample in order to probe only the vapor itself. Data points represent 6-pulse averages with the exception [Fig. 4(e)] of the background measurements on the bare silica substrate (60-pulse averages) and the vapor measurements (270-pulse averages). The measured background laser scatter [open circles in Fig. 4(e)] from the bare silica substrate was small but measurable above the detector dark counts. The signal was less than 0.1 photon per pulse (~0.03 photon/pulse at 236.2 nm), and when plotted on a log scale over a larger range of wavelengths (not shown), follows the steep slope of the interference filter. All explosive samples display the same multipeak structure with a maximum signal at the excitation wavelength of 236.2 nm and shoulder near 236.3 nm. They also display a secondary peak at 236.9 nm, again with an accompanying shoulder. An estimate of the signal-to-noise ratio for the detection process can be made by comparing the background laser scatter (no explosive present) to the signal with explosive present. For TNT at 236.2 nm, this yields a signal-to-noise ratio of $10/0.03 = 333$ (25 dB). It is noted that the vapor pressures for these compounds differ by over four orders of magnitude at room temperature (see Table 1), while the signals measured when probing the solids or liquids directly [Figs. 4(a)–4(d)] are within one order of magnitude, indicating that this signal is not related to the ambient vapors of the materials but rather to the condensed phase itself. To further test this conclusion, we probed the head space above DNT (the compound with the highest vapor pressure). The signal above the solid DNT was nonexistent (at or below the dark count rate of our detector). When the sample was liquefied (thus increasing its vapor pressure significantly), a response was measured [Fig. 4(e)] that was roughly 1% of the signal obtained by probing the liquid directly. These vapor phase

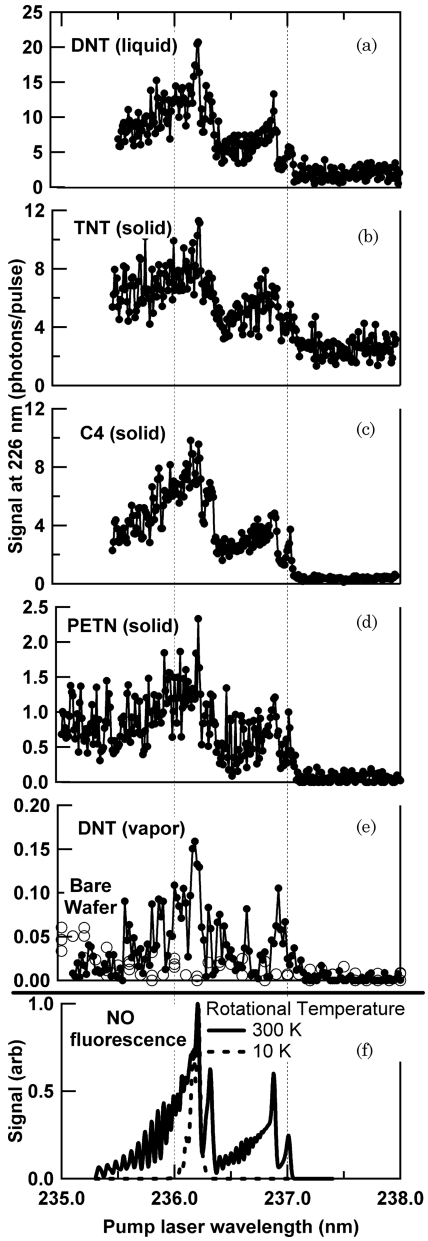

Fig. 4. Blue-shifted fluorescence signal of various explosives as a function of pump laser wavelength. (a)–(d) The laser beam directly strikes the explosives (solid or liquid). (e) The open circles are a background measurement in which the laser strikes the silica substrate without explosives, and the closed circles are a measurement in which the laser probes only the vapor headspace above liquid DNT (but not the liquid itself). (f) The predicted fluorescence of NO assuming excitation from its first vibrationally excited state; two different rotational temperatures are displayed.

results are consistent with expectations based on the known vapor pressures of DNT. As the temperature of DNT is raised from 300 K to its melting point near 70 C, its vapor pressure is expected to increase by a factor of 25 to 5000 ppb [7]. Thus we would expect the signal generated by the vapor above the solid at 300 K to be a factor of 25 smaller than the signal generated by the vapor above the liquid or roughly 0.006 photons/pulse, which is below our detection limits. Furthermore, the fact that the signal due to the vapor above the liquid is ~1% that of the signal generated by the liquid itself can be understood by estimating the number of molecules interrogated in each case. As shown later in this section, we estimate that 5×10^{13} molecules are interrogated when the liquid is probed directly. When the vapor is probed directly, we assume a 0.1 cm^2 spot over a 0.5 cm path length with a DNT partial pressure that is 10% that of its saturated partial pressure of 5000 ppb (due to atmospheric mixing), yielding 7.5×10^{11} molecules interrogated. This is roughly 1% of the amount interrogated via direct liquid probe, consistent with our experimental results.

Figure 4(f) displays the predicted fluorescence spectrum of NO assuming excitation from the first vibrationally excited state ($v'' = 1$) of its electronic ground state ($X^2\Pi$) to the vibrational ground state ($v' = 0$) of its first electronically excited state ($A^2\Sigma$) at two different rotational temperatures. These results were obtained using the LIFBASE software package [8,9]. The LIFBASE package allows the user to independently alter translational, vibrational, and rotational temperatures; it also allows a user-defined linewidth. Our calculations assumed a linewidth of 0.03 nm to match our laser bandwidth. Comparison of the experimental data to the NO spectrum provides clear evidence that the measured signal is generated by an excited NO species. Furthermore, the width of the spectra argues for an effective rotational temperature that is at least 300 K. A more careful analysis of the spectra at different rotational temperatures indicates the excited ($v'' = 1$) NO has an effective rotational temperature of 1000 + / – 500 K, for which two primary bandheads separated by 0.7 nm (related to the two spin states of the NO electronic ground state) are populated. Note that this temperature is somewhat fluence- and morphology-dependent (as discussed later in this section). A rotational temperature of ~1000 K is in contrast to previous PD-LIF results on RDX vapors [10], for which the effective rotational temperature was observed to be 20 K, but is closer to results of resonantly enhanced multiphoton ionization (REMPI) studies of solid RDX for which the rotational temperature of the NO fragment was estimated to be 325 K [11]. The fact that the rotational temperature in the REMPI studies is still lower than in our studies may be attributed to the different time scales of the two measurements. The REMPI studies were conducted on a significantly longer timescale (millisecond) than the present measurements (nanosecond), possibly allowing for collisional equilibration of the molecular degrees of freedom as well as collisional cooling under the atmospheric ambient conditions.

For excitation wavelengths longer than 237 nm (too long to access the $v'' = 1$ state), there is still a measured fluorescence signal above the scattered light level. As discussed later in this section, this signal displays a nonlinear dependence on laser fluence, indicating that it is not laser scatter. Figure 5 dis-

plays a more complete excitation spectrum of the 226 nm fluorescence from liquid DNT at the laser fluence of 22 mJ/cm^2/pulse, spanning excitation from both $v'' = 1$ and $v'' = 2$. As is evident in Fig. 5, the signal above 237 nm is related to the rotational substructure of the $v'' = 2$ state. Comparison of the peak intensities near $v'' = 1$ (236.2 nm) and $v'' = 2$ (~247 nm) yields a relative ratio of 3:1. However, since rotational temperatures may vary with vibrational state (discussed later), the peak values may not be the best indicator of relative populations. Integration over all rotational states within +/− 1 nm of the peaks yields a relative ratio of 3.5:1. This is similar to the relative intensities of 5:1 measured in vapor DNT [6]. Estimates of the relative populations must be adjusted by the differing Franck–Condon factors for which $[X^2\Pi(v'' = 1) - A^2\Sigma(v'' = 0)]$ is 10% higher than $[X^2\Pi(v'' = 2) - A^2\Sigma(v'' = 0)]$, yielding a relative population estimate of 3.2:1 for $v'' = 1{:}2$.

The data near $v'' = 1$ fit the predicted NO fluorescence quite well for a rotational temperature of 1000 K, while the data near $v'' = 2$ can be better fit to a rotational temperature of 5000 K. Attempts to fit the signal originating from $v'' = 1$ and 2 to a common intermediate rotational temperature yielded a poorer fit for both states. By comparison a rotational temperature of 3500 K for the $v'' = 2$ excitation has been estimated based on PD-LIF measurements of vapor phase DNT [6]. The difference in our estimated rotational temperatures of $v'' = 1$ (1000 K) and $v'' = 2$ (5000 K) may indicate differences in their respective photodissociation processes. Studies of the photodissociation of NO_2 (a potential intermediate in our dissociation process) indicate

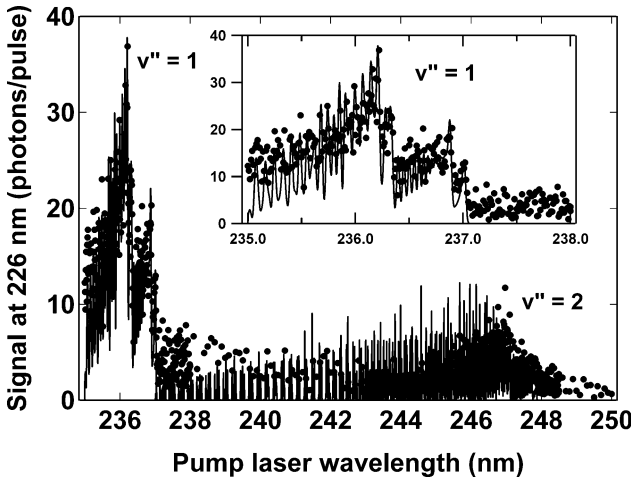

Fig. 5. Blue-shifted fluorescence signal of liquid DNT as a function of pump laser wavelength (22 mJ/cm^2/pulse). The markers are experimental data for liquid DNT, and the lines are the predicted NO fluorescence. The predicted NO fluorescence pumped at wavelengths below 237 nm is for excitation from $v'' = 1$ with a rotational temperature of 1000 K. The predicted NO fluorescence pumped at wavelengths above 237 nm is for excitation from $v'' = 2$ with a rotational temperature of 5000 K. The inset is a close-up near $v'' = 1$.

clear differences in the dissociation mechanisms for different wavelength regimes (220–226 nm versus 227–237 nm) [12], and we surmise that they may again be different at 237–250 nm.

Photolysis rates were measured at 236.2 nm by counting the number of pulses required to photolyze a thin film of known thickness. For TNT a photolysis rate of 28 nm/pulse (at 25 mJ/cm^2/pulse) was estimated for a millimeter thick film. Additionally, TNT diluted in acetone was used to create a dropcast film on a silicon wafer with an aerial coverage of 2 μg/cm^2. The measured signal for this film was roughly half that of the bulk sample. Approximately ten laser pulses at 10 mJ/cm^2/pulse (0.1 cm^2 spot size) were required to fully ablate the dropcast film, as was evident not only by eye but also by the measured fluorescence signal [13]. Based on these results we can estimate that in our specific experimental configuration, we were detecting 20 ng TNT with each laser pulse.

For DNT a photolysis rate of 23 nm/pulse (at 28 mJ/cm^2/pulse) was measured for a bulk sample. Assuming a linear fluence dependence (discussed later), the photolysis rate of DNT at 25 mJ/cm^2/pulse is ~20 nm/pulse. Therefore, at the fixed fluence of 25 mJ/cm^2/pulse, the ratio of the photolysis rates of TNT and DNT is ~28:20 = 1.4, which is close to the ratio of the molecular absorption cross sections at 236 nm (7.7×10^{-17} cm^2/molec: 5.0×10^{-17} cm^2/molec, see Table 1). Certainly the photolysis rates of TNT and DNT do not follow their respective vapor pressures, which differ by a factor of ~13 in the "wrong direction" (i.e., the vapor pressure of DNT is higher while its photolysis rate is somewhat lower than that of TNT). This behavior is a strong indication that the fluorescence originates from the respective condensed phases.

It is evident from the basic mechanism of PD-LIF that more than one photon is involved in the generation of each NO photofragment. Therefore it is to be expected that the observed fluorescence will display a nonlinear dependence on laser fluence. Our experiments validate this prediction, but they also display a more complex behavior, which varies from compound to compound and with wavelength. Figure 6 displays the fluorescence signal as a function of laser fluence for various explosives at various fixed laser wavelengths. Data points are averages over a number of samples, the amount of which depended upon the signal strength. In order to ensure that no systematic drift affected the measurements, the fluence was decreased to its minimum and then subsequently increased. All measurements were recorded at a fixed spot size of 0.1 cm^2 with the exception of the liquid DNT data. In order to achieve the higher fluences achieved in those measurements, the spot size was decreased by a factor of 4. Overlap between the two data sets spanned 1–40 mJ/cm^2 and was quite good after adjustment for the smaller spot size (the signal level of the high fluence data was multiplied by 4 in order to simulate a larger spot size

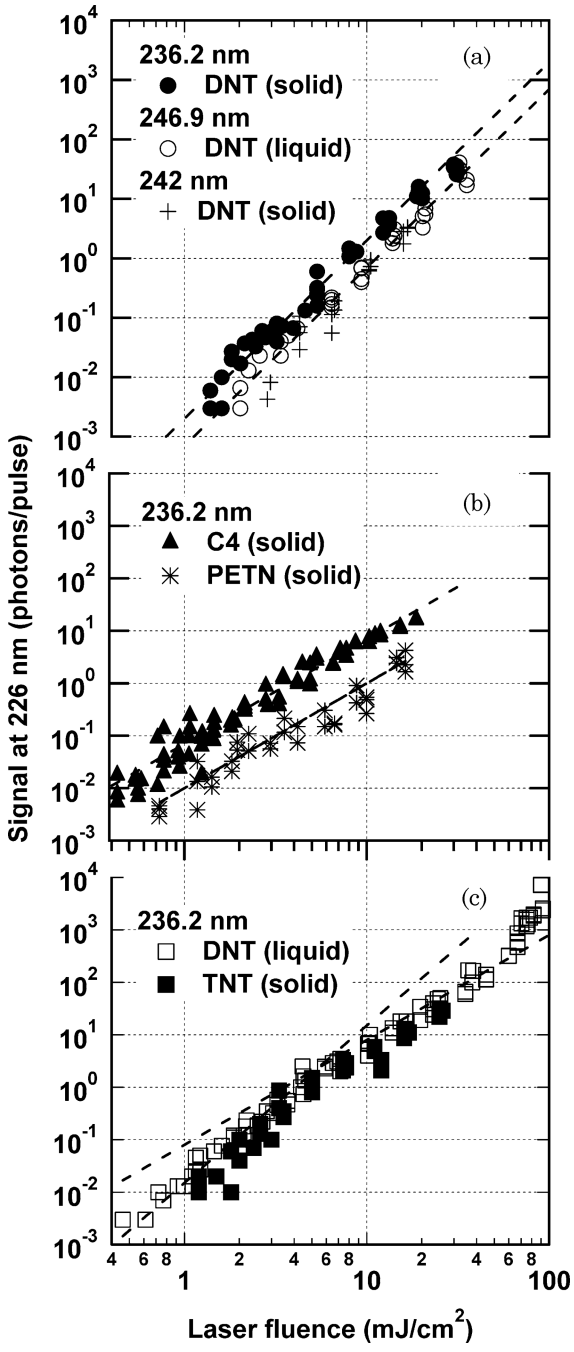

Fig. 6. Fluence dependence of the fluorescence signal of various explosives at fixed pump laser wavelengths. Dashed curves indicate either (a) cubic or (b) quadratic behavior. In (c) both quadratic and cubic behavior are indicated.

consistent with the other measurements). A number of different fluence dependencies are observed, dependent on the material, its physical phase (solid or liquid), and the laser wavelength. For laser irradiation at 236.2 nm, both liquid DNT and solid TNT show similar behavior, in which there appears to be a cubic dependence at low laser fluences crossing over to a quadratic dependence at higher fluences. At very high fluences (>60 mJ/cm^2/pulse), DNT displays a systematic shift by roughly a factor of 2 above its quadratic behavior below 60 mJ/cm^2/pulse. In contrast, cubic dependence on fluence is observed in solid DNT (all wavelengths) and liquid DNT in which the $v'' = 2$ state is being probed (246.9 and 242 nm). Both C4 (the active component being RDX) and PETN display quadratic dependencies on laser fluence over the full range of our experimental conditions.

Other properties, in addition to the magnitude of the fluorescence signal, were also observed to vary with laser fluence. For solid DNT the photolysis rate varied from 23 nm/pulse (at 28 mJ/cm^2/pulse) to 4 nm/pulse (at 5 mJ/cm^2/pulse). Laser fluence also affected the rotational temperature. Figure 7 displays results for liquid DNT. Two regimes appear evident. For fluences below approximately 8 mJ/cm^2/pulse, the rotational temperature best matches predictions at 500 K, while above 8 mJ/cm^2/pulse the rotational temperature increases to ~1000 K.

The cubic fluence dependencies observed in DNT and TNT at low fluences may be interpreted in different ways. One relies on the suggestion [6] that the formation of NO fragments from a toluene derivative requires two photons, in which initial NO_2 fragments formed via the first photon are subsequently dissociated into NO + O via the second photon. In support of this interpretation, we note that indeed in our studies RDX does not display a cubic fluence dependence, and RDX has been shown to photodissociate directly into NO [14,15]. Alternatively the cubic dependence in DNT and TNT can be attributed to the dependence of the vaporization step, which was observed to increase in a roughly linear manner with fluence in DNT, and would affect the amount of vapor that could be accessed by the subsequent probe photons. This may be the more likely explanation, especially in light of the PD-LIF data from vapor phase DNT, which show a quadratic fluence dependence from ~1–7 mJ/cm^2/pulse [6].

The crossover from cubic to quadratic dependence for liquid DNT and solid TNT near 5 mJ/cm^2/pulse indicates the saturation of one of the optical processes. This is also near the point above which we observe the rotational temperature crossing to a higher value. The behavior of DNT at very high fluences (above 60 mJ/cm^2/pulse) may be related to the dissociation and/or excitation of its second nitro group.

The initial physical phase of DNT (solid versus liquid) clearly affects the resultant PD-LIF fluorescence. The fluorescence signal at the peak, 236.2 nm, is greater in the liquid phase than in the solid phase and also displays a different fluence dependence. This may be due in part to differences in vapor pressures. DNT has the highest vapor pressure of the materials measured (Table 1), and as such, the relative portion of its signal due to its vapor (prior to photovaporization/photodissociation) is likely to be the largest of the materials measured. Furthermore, the vapor pressure of DNT increases significantly as

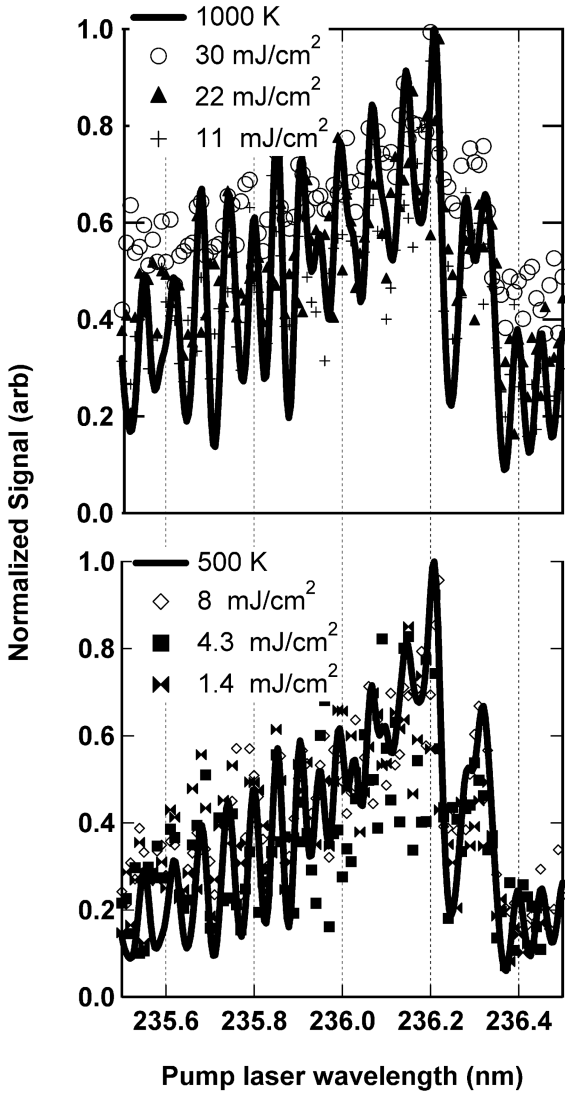

Fig. 7. Blue-shifted fluorescence signal of liquid DNT as a function of pump laser wavelength at various laser fluences. Signals have been normalized to their peak values at 236.2 nm. Symbols are experimental data, while the curves are predicted NO fluorescence for two different rotational temperatures.

its temperature is raised from 25 °C to its melting point just below our liquid measurements at 80 °C. Note, however, that the rotational temperature also changes depending on the phase of the DNT. Our measurements near $v'' = 1$ at a fluence of 1.9 mJ/cm^2/pulse indicate a rotational temperature of 500 K for the liquid phase and a rotational temperature of 2000 K for the solid phase. The integrated fluorescence over all wavelengths (near $v'' = 1$) remains larger by at least the same ratio as the fluorescence peaks, despite the higher rotational temperature of the solid. In general we observe that as the initial phase of DNT changes from liquid to solid, the rotational temperature increases, and the magnitude of the fluorescence at the peak of 236.2 nm decreases.

The fluence dependence of the DNT peaks differs depending on the excitation wavelength (near 236.2 or 247 nm), and once again there is a correlation with rotational temperature, which varies with excitation wavelength (see Fig. 5). Such correlations suggest differences in the dissociation physics as the excitation wavelength is varied over the different vibrational levels. Quantum-chemical simulations of the decomposition of RDX indicate that the energy required to cleave its N–NO_2 bonds is greater in the solid than in the vapor [16]. These same studies show that the energy barriers differ depending on the particular N–NO_2 group in the solid but not in the vapor. Similar effects may help explain our observed dependencies in DNT.

Previous studies indicate a higher PD-LIF fluorescence signal in RDX as compared to TNT [17]. The nature of the R–NO_2 bond was considered to be of primary importance in explaining these differences in that the R–NO_2 bond scission energy is higher in TNT (R = C) than RDX (R = N). Our low fluence data are consistent with these earlier studies. However, the fluence dependence is very different for the two species, and above 5 mJ/cm^2/pulse (at which point some saturation is occurring in TNT), the two signals are fairly similar. Additionally we observe that PETN (R = O), for which the R–NO_2 bond scission energy is expected to be the weakest [18], displays the weakest fluorescence in contrast to expectations based solely on R–NO_2 bond scission energy. Additional factors may be relevant in the case of PETN, such as its lower absorption coefficient at 236 nm (Fig. 3 and Table 1).

Finally, keeping in mind the eventual application of PD-LIF to the standoff detection of these compounds, it is important to calculate the relative efficiency of this process compared to the alternative of Raman spectroscopy. (While comparison to LIBS is also possible, PD-LIF and Raman-based detection have, in principle, similar low false alarm rates.) The Raman cross section for TNT has been reported as 2×10^{-31} cm^2/sr/molec for visible excitation and 10^{-28} cm^2/sr/molec for UV resonant excitation [19,20], and therefore the angle-integrated values are 2.5×10^{-30} and 10^{-27} cm^2/molec, respectively.

The spontaneous Raman scattering process is linear in fluence, and therefore the cross section is a constant. In contrast the PD-LIF is nonlinear in fluence, as amply discussed earlier. A "cross section" will therefore be fluence dependent, and furthermore it will be an effective parameter rather than a true molecular property. By analogy to a linear process such as Raman scattering, the number of fluorescence photons collected in our experimental setup, N_{photon}, can be expressed as follows:

$$N_{\text{photon}} = Fn\sigma_{\text{eff}}\eta. \quad (1)$$

In Eq. (1), F is the laser fluence (in photons per unit area), n is the number of molecules being irradiated, σ_{eff} is the effective cross section of the overall PD-LIF process, and η is the experimental collection efficiency. Besides being fluence dependent, σ_{eff} is also

the product of several molecular parameters:

$$\sigma_{\text{eff}} = \sigma_{\text{abs}}\eta_{\text{NO}}\sigma_{\text{exc}}\sigma_{\text{fl}}. \quad (2)$$

In Eq. (2), σ_{abs} is the absorption cross section per molecule, η_{NO} is the efficiency of forming a NO fragment in the appropriate $X^2\prod(v'' = 1)$ vibrational state, σ_{exc} is the probability of photoexcitation of a nascent NO fragment to the $A^2\Sigma(v' = 0)$ state, and σ_{fl} is the probability of fluorescent decay of the excited NO to the $X^2\prod(v'' = 0)$ state. While some of the figures defining σ_{eff} in Eq. (2) can be numerically identified, the magnitude of others is less certain. For the purpose of our estimate, we will leave them all lumped together in the value of σ_{eff}.

We estimate σ_{eff} based on our results at a fluence F of $10\,\text{mJ/cm}^2\text{/pulse}$ (1.25×10^{16} photons/cm^2). At this fluence, N_{photon} is ~10 photons/pulse [Fig. 6(c), TNT). The number of irradiated molecules, n, is obtained from dropcast TNT measurements for which the aerial density of the dropcast TNT is $2\,\mu\text{g/cm}^2$, the laser spot size is $0.1\,\text{cm}^2$, and the molecular weight of TNT is 227 g/mol. Noting that ~10 laser pulses were required to fully photolyze the film and that the total number of molecules in the film was 5×10^{14}, we estimate $n = 5 \times 10^{13}$ molecules/pulse. Note that the *average* thickness of the dropcast TNT is ~12 nm (the density of TNT is $1.65\,\text{g/cm}^3$), similar to our measured photolysis rate per pulse. However, experimentally we observed that 10 pulses were required to photolyze the film, rather than one pulse, as may be indicated by the average film thickness. These results are reconciled by noting, as is evident from optical images of the films, that the films are not uniform, but rather they consist of islands of different sizes and presumably thicknesses. Using the value of η as 4×10^{-7} (Section 2), we obtain $\sigma_{\text{eff}} = 4 \times 10^{-23}\,\text{cm}^2\text{/molec}$ for TNT at a $10\,\text{mJ/cm}^2\text{/pulse}$ fluence. This is a factor of 4×10^4 higher than that achievable with Raman scattering in the optimal condition of UV excitation and ~10^7 higher than the more conventional visible–near-IR Raman scattering. Making the simplified assumption that the number of molecules probed via PD-LIF is fixed at $n = 5 \times 10^{13}$ molecules/pulse, we can use Eq. (1) and the TNT data of Fig. 4(c) to estimate the fluence dependence of σ_{eff}. This is compared to the Raman cross section, which remains fixed with fluence, in Fig. 8. As can be seen from Fig. 8, PD-LIF compares favorably with Raman scattering as a process enabling standoff detection of TNT and other nitro-bearing explosives.

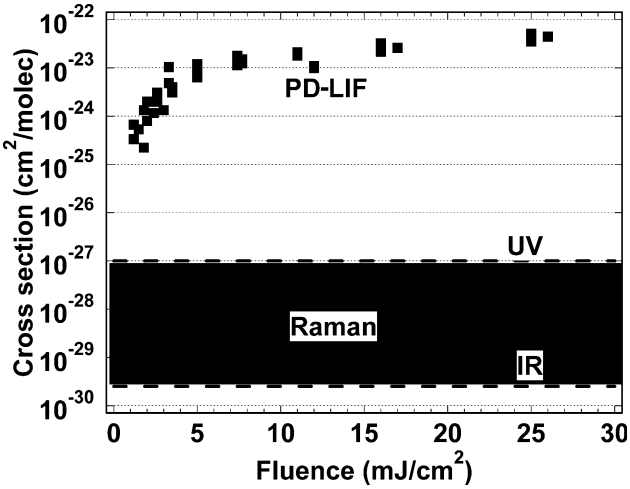

Fig. 8. TNT cross section as a function of fluence for PD-LIF (squares) and Raman detection (upper and lower bounds denoted by dashed lines). The Raman cross sections are from [19,20]. Note PD-LIF cross section estimates assume that the number of particles probed per pulse was constant with fluence and equal to the measured value at $10\,\text{mJ/cm}^2$.

4. Conclusions

A fully optical PD-LIF-based technique was used to detect various condensed-phase nitro-bearing explosives, including DNT, TNT, RDX, and PETN. Vibrationally excited NO fragments, obtained as a result of the laser interaction with the solids and liquid (as opposed to the ambient vapor), were clearly observed. Probing of the $v'' = 1$ state of the NO fragments yielded the largest signal-to-noise ratio. The resultant single-pulse fluorescent signal was ~25 dB above the background laser scatter at $10\,\text{mJ/cm}^2$/pulse. This fluorescent signal, which could potentially be utilized to detect trace amounts of explosives in a remote manner, depends on laser wavelength, laser fluence, material phase, and type of explosive molecule.

We thank the referee for insightful suggestions regarding the vapor headspace measurements. This work was sponsored under the auspices of the Lincoln Laboratory New Technologies Initiative Board (NTIB) Program. The NTIB Program is supported principally by the Department of the Air Force under contract FA8721-05-C-0002. Opinions, interpretations, conclusions, and recommendations are those of the authors and do not necessarily represent the view of the United States Government.

References

1. D. S. Moore, "Instrumentation for trace detection of high explosives," Rev. Sci. Instrum. **75**, 2499–2512 (2004).
2. S. Singh, "Sensors—An effective approach to the detection of explosives," J. Hazard. Mater. **144**, 15–28 (2007).
3. T. Arusi-Parpar, D. Helfinger, and R. Lavi, "Photodissociation followed by laser-induced fluorescence at atmospheric pressure and 20 C: a unique scheme for remote detection of explosives," Appl. Opt. **40**, 6677–6681 (2001).
4. D. Helfinger, T. Arusi-Parpar, Y. Ron, and R. Lavi, "Application of a unique scheme for remote detection of explosives," Opt. Commun. **204**, 327–331 (2002).
5. T. Arusi-Parpar and Izhak Levy, "Remote detection of explosives by enhanced pulsed laser photodissociation/laser-induced fluorescence method," *Standoff Detection of Suicide Bombers and Mobile Subjects*, H. Schubert and A. Rimski-Korsakow, eds. (Springer, 2006), pp. 59–68.

6. J. Shu, I. Bar, and S. Rosenwaks, "The use of rovibrationally excited NO photofragments as trace nitrocompound indicators," Appl. Phys. B **70**, 621–625 (2000).
7. C. Lenchitz and R. Velicky, "Vapor pressure and heat of sublimation of three nitrotoluenes," J. Chem. Eng. Data **15**, 401 (1970).
8. J. Luque and D. R. Crosley, "LIFBASE: database and spectral simulation program," SRI International Report MP 99-009 (1999).
9. J. Luque and D. R. Crosley, "Transition probabilities and electronic transition moments of the $A^2\sum^+ - X^2\Pi$ and $D^2\sum^+ - X^2\Pi$ systems of nitric oxide" J. Chem. Phys. **111**, 7405 (1999).
10. Y. Q. Guo, M. Greenfield, and E. R. Bernstein, "Decomposition of nitramine energetic materials in excited electronic states: RDX and HMX," J. Chem. Phys. **122**, 244310 (2005).
11. J. Cabalo and R. Sausa, "Detection of RDX by laser surface photofragmentation-fragment detection spectroscopy," Appl. Spectrosc. **57**, 1196–1199 (2003).
12. H.-S. Im and E. R. Bernstein, "Photodissociation of NO_2 in the region 217–237 nm: Nascent NO energy distribution and mechanism," J. Phys. Chem. A **106**, 7565–7572 (2002).
13. C. M. Wynn, S. Palmacci, R. R. Kunz, J. J. Zayhowski, B. Edwards, and M. Rothschild, "Experimental demonstration of remote detection of trace explosives," Proc. SPIE **6954**, 695407 (2008).
14. M. Greenfield, Y. Q. Guo, and E. R. Bernstein, "Ultrafast photodissociation dynamics of HMX and RDX from their excited electronic states via femtosecond laser pump-probe techniques," Chem. Phys. Lett. **430**, 277–281 (2006).
15. H. S. Im and E. R. Bernstein, "On the initial steps in the decomposition of energetic materials from excited electronic states," J. Chem. Phys. **113**, 7911–7918 (2000).
16. M. Kuklja, "Thermal decomposition of solid cyclotrimethylene trinitramine," J. Phys. Chem. B **105**, 10159–10162 (2001).
17. J. Cabalo and R. Sausa, "Trace detection of explosives with low vapor pressure emissions by laser surface photofragmentation-fragment detection spectroscopy with an improved ionization probe," Appl. Opt. **44**, 1084–1091 (2005).
18. F. J. Owens, "Calculation of energy barriers for bond rupture in some energetic molecules," J. Mol. Struct., Theochem **370**, 11–16 (1996).
19. L. Nagli and M. Gaft, "Raman scattering spectroscopy for explosives identification," Proc. SPIE **6552**, 65502Z (2007)
20. M. Gaft and L. Nagli, "UV gated Raman spectroscopy for standoff detection of explosives," Opt. Mater. **30**, 1747–1754 (2008).
21. National Research Council, *Existing and Potential Standoff Explosive Detection Techniques* (National Academies, 2004).
22. J. Steinfeld and J. Wormhoudt, "Explosives detection: a challenge for physical chemistry," Annu. Rev. Phys. Chem. **49**, 203–232 (1998).
23. A. Gonzalez, C. Larson, D. McMillen, and D. Golden, "Mechanism of decomposition of nitroaromatics. Laser-powered homogeneous pyrolysis of substituted nitrobenzenes," J. Phys. Chem. **89**, 4809–4814 (1985).